

# Travelling solitons in the externally driven nonlinear Schrödinger equation

I. V. Barashenkov\*

*Department of Mathematics, University of Cape Town, Rondebosch 7701; and  
National Institute for Theoretical Physics, Stellenbosch, South Africa*

E. V. Zemlyanaya†

*Joint Institute for Nuclear Research, Dubna, 141980 Russia*

(Dated: April 21, 2022)

We consider the undamped nonlinear Schrödinger equation driven by a periodic external force. Classes of travelling solitons and multisoliton complexes are obtained by the numerical continuation in the parameter space. Two previously known stationary solitons and two newly found localised solutions are used as the starting points for the continuation.

We show that there are two families of stable solitons: one family is stable for sufficiently low velocities while solitons from the second family stabilise when travelling faster than a certain critical speed. The stable solitons of the former family can also form stably travelling bound states.

PACS numbers: 05.45.Yv

## I. INTRODUCTION

The damped nonlinear Schrödinger equation driven by a time-periodic external force,

$$iu_t + u_{xx} + 2|u|^2u + \delta u = ae^{i\Omega t} - i\beta u, \quad (1a)$$

and its parametrically driven counterpart model two fundamental energy supply mechanisms in a nearly-conservative spatially distributed system. While the unperturbed Schrödinger is an archetypal equation for the slowly varying envelope of a group of dispersive waves, the damped-driven equations arise whenever the resonant forcing of small amplitude is used to compensate weak dissipative losses.

The simplest (and perhaps the most visually appealing) realisation of Eq.(1a) is that of the amplitude equation for a strongly coupled pendulum array with the horizontal sinusoidal driving [1], taken in its continuum limit. Here  $a$  and  $\Omega$  are the driving strength and driving frequency, respectively;  $\delta$  is the detuning of the driving frequency from the continuum of linear waves in the array, and  $\beta$  is the damping coefficient.

The array of torsionally coupled pendula can serve as a prototype model for the whole variety of systems in condensed matter physics. Accordingly, Eq.(1a) was employed to study systems as diverse as the ac-driven long Josephson junctions [2] and charge-density-wave conductors with external electric field [3]; double-layer quantum Hall (pseudo)ferromagnets [4] and easy-axis ferromagnets in a rotating magnetic field [5]. Eq.(1a) arises in the theory of rf-driven waves in plasma [6, 7] and shear flows in nematic liquid crystals [8]; the same equation governs the amplitude of the slowly varying  $\pi$ -mode in the forced Fermi-Pasta-Ulam lattice [9].

A closely related equation is the one with the *spatially* periodic forcing,

$$iu_t + u_{xx} + 2|u|^2u + \delta u = ae^{iKx} - i\beta u, \quad (1b)$$

and, more generally, the one driven by the harmonic wave [10–12]:

$$iu_t + u_{xx} + 2|u|^2u + \delta u = ae^{i(Kx+\Omega t)} - i\beta u. \quad (1c)$$

A discrete version of Eq.(1b) describes an array of coupled-waveguide resonators excited by a driving field [13] whereas Eq.(1c) models pulse propagation in an asymmetric twin-core optical fiber [10].

Equation (1c) includes (1a) and (1b) as particular cases. The transformation

$$u(x, t) = \Psi(X, t)e^{i(Kx+\Omega t)}, \quad X = x - 2Kt$$

takes (1c) to

$$i\Psi_t + \Psi_{XX} + 2|\Psi|^2\Psi - \kappa^2\Psi = a - i\beta\Psi, \quad (2)$$

with  $\kappa^2 = K^2 + \Omega - \delta$ . The equation in this form has a history of applications of its own — in particular, in the physics of optical cavities. Originally, it was introduced as the Lugiato - Levefer model [14] of the diffractive cavity driven by a plane-wave stationary beam. Later it was employed to describe a synchronously pumped ring laser with a nonlinear dispersive fiber [15, 16]. More recently the same equation was shown to govern the envelopes of short baroclinic Rossby waves in the two-layer model of the atmosphere, or the ocean [17].

Equation (2) has undergone an extensive mathematical analysis. Topics covered included existence [18, 20, 21], stability [20, 22] and bifurcation [7, 19] of nonpropagating solitons and their bound states [16, 23–25]; statistical mechanics of soliton creation and annihilation [26]; soliton autoresonance phenomena [12, 27]; regular [28] and chaotic [29] attractors on finite spatial intervals. Here

\* Email: igor.barashenkov@gmail.com

† Email: elena@jinr.ru

and below we use the word “soliton” simply as a synonym for “localised travelling wave”.

The recent paper [30] studied solitons of the undamped ( $\beta = 0$ ) equation (2) travelling with constant or oscillating velocities. Summarising results of their direct numerical simulations of Eq.(2), the authors formulated an empirical stability criterion of the soliton against small and large perturbations. So far, this criterion has not been given any mathematical proof or physical justification. Despite being tested on a variety of initial conditions, it still has the status of conjecture.

In order to verify the validity of the empirical stability criterion at least for infinitesimal perturbations, one needs to have the travelling soliton existence and linearised stability domains accurately demarcated. The classification of bifurcations occurring when stability is lost would also be a useful step towards the justification of the criterion. This is what we shall concern ourselves with in this paper.

Here, we study travelling solitons of Eq.(2) by path-following them in the parameter space. One advantage of this approach over simulations is that it furnishes *all* soliton solutions moving with a given velocity — all stable and all unstable. This, in turn, allows one to understand the actual mechanisms and details of the soliton transformations.

The outline of this paper is as follows. In the next section, we give a brief classification of space- and time-independent solutions of Eq.(2) which may serve as the backgrounds for the solitons. In particular, we show that there is only one stable background and determine the value of the limit speed of the soliton propagating over it. In section III we describe insights one can draw from the analysis of the eigenvalues of the symplectic linearised operator and its hermitian counterpart. These pertain to the stability and bifurcation of the solitons.

In section IV we present four *nonpropagating* directly driven solitons. Two of these have already been available in literature while the other two have not been known before. In sections V and VI, we report on the continuation of these stationary solitons to nonzero velocities. Our results on the existence and stability of the travelling solitons and their complexes, are summarised in section VII. In particular, Fig.8 gives a chart of “stable” velocities for each value of the driving strength.

## II. FLAT SOLUTIONS

Assuming that  $\kappa^2 > 0$  and defining  $t' = \kappa^2 t$ ,  $x' = \kappa X$ , and  $\Psi = \kappa \psi$ , equation (2) becomes

$$i\psi_{t'} + \psi_{x'x'} + 2|\psi|^2\psi - \psi = -h - i\gamma\psi,$$

where  $h = -a/\kappa^3$ ,  $\gamma = \beta/\kappa^2$ . (In what follows, we omit primes above  $x$  and  $t$  for notational convenience.)

In this paper we study the above equation with zero damping:  $\gamma = 0$ . Without loss of generality we can assume that  $h > 0$ . Since we shall be concerned with soli-

tons travelling at nonzero velocities, it is convenient to transform the equation to a co-moving frame:

$$i\psi_t - iV\psi_\xi + \psi_{\xi\xi} + 2|\psi|^2\psi - \psi = -h, \quad (3)$$

where  $\xi = x - Vt$ .

Flat solutions are roots of the cubic equation

$$2|\psi|^2\psi - \psi = -h; \quad (4)$$

these have been classified in [20]. If  $0 < h < (2/27)^{1/2}$ , there are 3 roots, of which two ( $\psi_1$  and  $\psi_2$ ) are positive, and one ( $\psi_3$ ) is negative. Here  $\psi_1^2 < \frac{1}{6} < \psi_2^2 < \frac{1}{2} < \psi_3^2 < \frac{2}{3}$ . If  $h > (2/27)^{1/2}$ , there is only one (negative) solution  $\psi_3$ , with  $\psi_3^2 > \frac{2}{3}$ .

Let  $\psi_0$  denote a root of equation (4) — one of the three roots  $\psi_1$ ,  $\psi_2$  and  $\psi_3$ . The value  $\psi_0$  does not depend on  $V$ : the flat solution has the same form in any frame of reference. However the spectrum of small perturbations of the flat solution does include a dependence on  $V$ . Letting  $\psi = \psi_0 + [u(\xi) + iv(\xi)]e^{\lambda t}$  in (3), linearising in  $u$  and  $v$ , and, finally, taking  $u, v \propto e^{ik\xi}$ , we obtain

$$(\lambda - ikV)^2 = -(k^2 + a^2)(k^2 + b^2), \quad (5)$$

where we have introduced

$$a = \sqrt{1 - 6\psi_0^2}, \quad b = \sqrt{1 - 2\psi_0^2}. \quad (6)$$

To determine whether  $\psi_0$  can serve as a background to a stationary localised solution of (3), consider a time-independent perturbation — that is, set  $\lambda = 0$ :

$$k^2 V^2 = (k^2 + a^2)(k^2 + b^2). \quad (7)$$

The only flat solution that is *a priori* unsuitable as a background for localised solutions is such  $\psi_0$  whose associated quadratic equation (7) has two nonnegative real roots,  $(k^2)_1 \geq 0$  and  $(k^2)_2 \geq 0$ .

It is not difficult to check that the negative solution  $\psi_3$  has two nonnegative roots for any choice of  $h$  and  $V$ . This disqualifies  $\psi_3$  as a possible soliton background. We also conclude that travelling solitons may not exist for  $h$  greater than  $(2/27)^{1/2}$ .

Next, if  $V \leq c$ , where

$$c = a + b, \quad (8)$$

the smaller positive solution  $\psi_1$  will have either two complex or two negative roots  $(k^2)_{1,2}$ , whereas for velocities greater than  $c$ , both roots are nonnegative. Hence the  $\psi_1$  solution can serve as a background only for  $V \leq c$ . When  $V < b - a$ , the decay to the background is monotonic (both roots are negative), while when  $V > b - a$ , the decay is by oscillation (the roots are complex). This flat solution admits a simple explicit expression:

$$\psi_1 = \sqrt{\frac{2}{3}} \cos\left(\frac{\alpha}{3} - \frac{2\pi}{3}\right),$$

where

$$\alpha = \arccos\left(-\sqrt{\frac{27}{2}}h\right), \quad \frac{\pi}{2} \leq \alpha \leq \pi.$$

Finally, the larger positive solution  $\psi_2$  has two real roots of opposite signs (for all  $V$  and  $0 \leq h \leq (2/27)^{1/2}$ ). This flat solution may also serve as a soliton background.

Next, one can readily check that a flat solution  $\psi_0$  is stable if  $\psi_0^2 < \frac{1}{6}$ . Therefore, even if there are solitons asymptotic to the flat solution  $\psi_2$  as  $x \rightarrow \infty$  or  $x \rightarrow -\infty$ , these will be of little physical interest as the background  $\psi_2$  is always unstable.

In summary, only the small positive flat solution (the one with  $\psi_0^2 < \frac{1}{6}$ ) is stable. It may serve as a background for solitons only if  $V < c$ ; that is, the soliton propagation speed is limited by  $c$ .

The inequality  $V \leq c$  limiting the soliton propagation speed, has a simple physical interpretation. Indeed, one can easily check that  $c$  gives the lower bound for the phase velocity of radiation waves [in the original  $(x, t)$  reference frame]. Therefore, a soliton travelling faster than  $c$  would be exciting resonant radiation. This is inconsistent with the asymptotic behaviour  $\psi_x \rightarrow 0$  as  $|x| \rightarrow \infty$ ; neither could it be reconciled with the energy conservation.

### III. INSIGHTS FROM LINEARISATION

Travelling wave solutions depend on  $x$  and  $t$  only in combination  $\xi = x - Vt$ . For these, the partial differential equation (3) reduces to an ordinary differential equation

$$-iV\psi_\xi + \psi_{\xi\xi} + 2|\psi|^2\psi - \psi = -h. \quad (9)$$

It is this equation that we will be solving numerically in the following sections.

Let  $\psi_s(\xi)$  be a localised solution of (9). In order to represent results of continuation graphically, we will need to characterise the function  $\psi_s(\xi)$  by a single value. A convenient choice for such a bifurcation measure is the momentum integral

$$P = \frac{i}{2} \int (\psi_\xi^* \psi - \psi_\xi \psi^*) d\xi. \quad (10)$$

One advantage of this choice is that the momentum is an integral of motion for equation (3); hence  $P$  is a physically meaningful characteristic of solutions. Another useful property of the momentum is that in some cases its extrema mark the change of the soliton stability properties (see below).

#### A. The hermitian and symplectic operator

Many aspects of the soliton's bifurcation diagram can be explained simply by the behaviour of the eigenvalues of the operator of linearisation about the travelling-wave

solution in question. Therefore, before proceeding to the numerical continuation of travelling waves, we introduce the linearised operator and discuss some of its properties.

Consider a perturbation of the solution of Eq.(9) of the form  $\psi = \psi_s + [u(\xi) + iv(\xi)]e^{\lambda t}$ , with small  $u$  and  $v$ . Substituting  $\psi$  in Eq. (3) and linearising in  $u$  and  $v$ , we get a symplectic eigenvalue problem

$$\mathcal{H}\vec{y} = \lambda J\vec{y}. \quad (11)$$

Here  $\vec{y}$  is a two-component vector-function

$$\vec{y}(\xi) = \begin{pmatrix} u \\ v \end{pmatrix},$$

and  $\mathcal{H}$  is a hermitian differential operator acting on such functions:

$$\mathcal{H} = \begin{pmatrix} -\partial_\xi^2 + 1 - 2(3\mathcal{R}^2 + \mathcal{I}^2) & -V\partial_\xi - 4\mathcal{R}\mathcal{I} \\ V\partial_\xi - 4\mathcal{R}\mathcal{I} & -\partial_\xi^2 + 1 - 2(3\mathcal{I}^2 + \mathcal{R}^2) \end{pmatrix},$$

with  $\mathcal{R}$  and  $\mathcal{I}$  denoting the real and imaginary part of the solution  $\psi_s(\xi)$ :  $\psi_s = \mathcal{R} + i\mathcal{I}$ . Finally,  $J$  is a constant skew-symmetric matrix

$$J = \begin{pmatrix} 0 & -1 \\ 1 & 0 \end{pmatrix}.$$

Assume that  $\psi_s(\xi)$  is a localised solution decaying to  $\psi_0$  as  $x \rightarrow \pm\infty$ , where  $\psi_0^2 < \frac{1}{6}$ . The continuous spectrum of the hermitian operator  $\mathcal{H}$  occupies the positive real axis with a gap separating it from the origin:  $E \geq E_0 > 0$ . Discrete eigenvalues  $E_n$  satisfy  $E_n < E_0$ . On the other hand, the continuous spectrum of the *symplectic* eigenvalues (that is, the continuous spectrum of the operator  $J^{-1}\mathcal{H}$ ) occupies the imaginary axis of  $\lambda$  outside the gap  $(-i\omega_0, i\omega_0)$ . The gap width here is given by

$$\omega_0 = \sqrt{(k_0^2 + a^2)(k_0^2 + b^2)} - Vk_0 > 0, \quad (12)$$

where  $k_0$  is the positive root of the bicubic equation

$$V^2(k^2 + a^2)(k^2 + b^2) = k^2(2k^2 + a^2 + b^2)^2.$$

Discrete eigenvalues of the operator  $J^{-1}\mathcal{H}$  may include pairs of opposite real values  $\lambda = \pm\rho$ ; pure imaginary pairs  $\lambda = \pm i\omega$ , with  $0 \leq \omega \leq \omega_0$ ; and, finally, complex quadruplets  $\lambda = \pm\rho \pm i\omega$ .

We routinely evaluate the spectrum of symplectic eigenvalues as we continue localised solutions in  $V$ . If there is at least one eigenvalue  $\lambda$  with  $\text{Re}\lambda > 0$ , the solution  $\psi_s$  is considered linearly unstable. Otherwise (that is, if all eigenvalues have  $\text{Re}\lambda \leq 0$ ), the solution is deemed linearly stable.

#### B. Zero eigenvalues

While the eigenvalues of the operator  $J^{-1}\mathcal{H}$  (that is, the eigenvalues of the symplectic eigenvalue problem

(11)) determine stability or instability of the solution  $\psi_s$ , the eigenvalues of the operator  $\mathcal{H}$  are significant for the continuability of this solution. Of particular importance are its zero eigenvalues.

At a generic point  $V$ , the operator  $\mathcal{H}$  has only one zero eigenvalue, with the translational eigenvector  $\vec{\Psi}_\xi \equiv (\mathcal{R}_\xi, \mathcal{I}_\xi)$ . This is due to the fact that the stationary equation (9) has only one continuous symmetry. For a given  $V$ , the solution  $\psi_s(\xi)$  is a member of a *one*-parameter family of solutions  $\psi_s(\xi - \theta)$ , where  $\theta$  is an arbitrary translation.

On the other hand, the nonhermitian operator  $J^{-1}\mathcal{H}$  has two zero eigenvalues at a generic point. The reason is that the equation (3) as well as its linearisation, are hamiltonian systems. Real and imaginary eigenvalues of operators which generate hamiltonian flows always come in pairs: If  $\mu$  is an eigenvalue, so is  $-\mu$  [33]. The two zero eigenvalues of the operator  $J^{-1}\mathcal{H}$  reflect the fact that the function  $\psi_s(\xi)$ , considered as a solution of the partial differential equation (3), is a member of a two-parameter family. One parameter is the translation; the other one is the velocity  $V$ .

For generic  $V$ , the repeated zero eigenvalue of  $J^{-1}\mathcal{H}$  is defective: there is only one eigenvector  $\vec{\Psi}_\xi$  associated with it. There is also a generalised eigenvector  $\vec{\Psi}_V$ , where

$$\vec{\Psi}_V \equiv \left( \frac{\partial \mathcal{R}}{\partial V}, \frac{\partial \mathcal{I}}{\partial V} \right).$$

This vector-function is *not* an eigenvector of  $J^{-1}\mathcal{H}$ ; instead, differentiating (9) in  $V$  one checks that  $\vec{z} = \vec{\Psi}_V$  satisfies the nonhomogeneous equation

$$\mathcal{H}\vec{z} = -J\vec{\Psi}_\xi. \quad (13)$$

[That is,  $\vec{\Psi}_V$  is an eigenvector of the *square* of the symplectic operator:  $(J^{-1}\mathcal{H})^2\vec{\Psi}_V = 0$ .]

As we continue in  $V$ , a pair of opposite pure-imaginary symplectic eigenvalues may collide at the origin on the  $\lambda$ -plane and cross to the positive and negative real axis, respectively. The algebraic multiplicity of the eigenvalue  $\lambda = 0$  increases from 2 to 4 at the point  $V = V_c$ ; however if the hermitian operator  $\mathcal{H}$  does not acquire the second eigenvalue  $E = 0$  at this point, the geometric multiplicity remains equal to 1. The change of stability of the soliton solution does not affect its continuability, i.e. the soliton exists on either side of  $V = V_c$ . In this case we have  $dP/dV = 0$  at the point where the stability changes [32].

The continuation may be obstructed only when another (the second) eigenvalue of the operator  $\mathcal{H}$  crosses through zero at  $V = V_c$ :  $\mathcal{H}\vec{\Phi} = 0$ . If the corresponding eigenvector  $\vec{\Phi}$  is not orthogonal to the vector-function  $J\vec{\Psi}_\xi$  in the right-hand side of equation (13), its solution  $\vec{z} = \vec{\Psi}_V$  will not be bounded. This implies a saddle-node bifurcation; the soliton solution  $\psi_s$  cannot be continued beyond  $V = V_c$ . Note that although  $\vec{\Phi}$  is an eigenvector of the symplectic operator  $J^{-1}\mathcal{H}$ , the algebraic multiplicity of the symplectic eigenvalue remains equal to 2 in this case.

Assume now that the eigenvector  $\vec{\Phi}$  is orthogonal to  $J\vec{\Psi}_\xi$ . This may happen if the soliton solution  $\psi_s$  of equation (9) with  $V = V_c$  is a member of a *two*-parameter family of solutions  $\psi_s = \psi_s(\xi - \theta; \chi)$ , with  $\chi$  equal to some  $\chi_0$ . Here we assume that *each* member of the family  $\psi_s(\xi - \theta; \chi)$  is a solution of Eq.(9) — with the same  $V = V_c$ . Then  $\vec{\Phi}$  is given by  $\vec{\Psi}_\chi \equiv \partial\vec{\Psi}/\partial\chi|_{\chi=\chi_0}$ . If  $\chi_0$  is a root of the equation

$$F(\chi) = 0, \quad (14a)$$

where

$$F(\chi) \equiv \int (\vec{\Psi}_\chi, J\vec{\Psi}_\xi) d\xi, \quad (14b)$$

the vectors  $\vec{\Psi}_\chi$  and  $J\vec{\Psi}_\xi$  will be orthogonal which, in turn, will imply that a bounded solution  $\vec{\Psi}_V$  of the equation (13) exists. [In Eq.(14b)  $(\ , \ )$  stands for the  $\mathbb{R}^2$  scalar product:  $(\vec{a}, \vec{b}) \equiv a_1b_1 + a_2b_2$ .] In this case the value  $V_0$  is *not* a turning point; the soliton solution  $\psi_s$  exists on both sides of  $V = V_0$ . The algebraic multiplicity of the zero symplectic eigenvalue increases at the point  $V = V_c$ . In fact from the hamiltonian property it follows that it increases up to 4 (rather than 3).

Recalling the definition of the momentum integral (10) and writing it in terms of the real and imaginary part of  $\psi_s$ , equation (14) becomes simply

$$\left. \frac{\partial P}{\partial \chi} \right|_{\chi=\chi_0} = 0.$$

This condition ensures that a two-parameter family of solutions  $\psi_s(x - \theta; \chi)$ , existing at the velocity  $V = V_0$ , has a one-parameter subfamily  $\psi_s(x - \theta; \chi_0)$  continuable to  $V \neq V_c$  [32].

## IV. NON-PROPAGATING SOLITONS

### A. Simple solitons

The ordinary differential equation (9) with  $V = 0$ ,

$$\psi_{xx} + 2|\psi|^2\psi - \psi = -h, \quad (15)$$

has two real-valued localised solutions,  $\psi_+$  and  $\psi_-$ . These are given by explicit formulas [22]:

$$\psi_\pm(x) = \psi_0 \left[ 1 + \frac{2 \sinh^2 \beta}{1 \pm \cosh \beta \cosh(Ax)} \right], \quad (16)$$

where the parameter  $\beta$  ( $0 \leq \beta < \infty$ ) is in one-to-one correspondence with the driving strength  $h$ :

$$h = \frac{\sqrt{2} \cosh^2 \beta}{(1 + 2 \cosh^2 \beta)^{3/2}}.$$

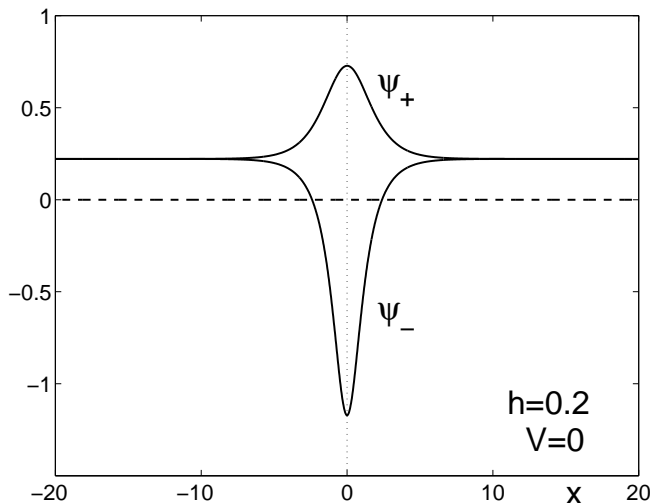


FIG. 1. Stationary  $\psi_+$  and  $\psi_-$  solitons

As  $h$  increases from 0 to  $\sqrt{2/27} \approx 0.2722$ ,  $\beta$  decreases from infinity to zero. (Hence  $0 \leq h \leq 0.2722$  is the domain of existence of the two solitons.) The asymptotic value  $\psi_0$  and inverse width  $A$  are also expressible through  $\beta$ :

$$\psi_0 = \frac{1}{\sqrt{2}} \frac{1}{\sqrt{1 + 2 \cosh^2 \beta}}, \quad A = \frac{\sqrt{2} \sinh \beta}{\sqrt{1 + 2 \cosh^2 \beta}}.$$

(Note that the asymptotic value  $\psi_0$  corresponds to the stable background, denoted  $\psi_1$  in Sec.II.)

The stationary soliton  $\psi_+$  has a positive eigenvalue in the spectrum of the linearised operator (11); hence the  $\psi_+$  is unstable for all  $h$  for which it exists [22]. The spectrum of the stationary soliton  $\psi_-$  with small  $h$  includes two discrete eigenvalues  $\lambda_{1,2} = i\omega_{1,2}$ ,  $\omega_{1,2} > 0$  — and their negative-imaginary counterparts. As  $h$  grows to 0.07749,  $\lambda_1$  and  $\lambda_2$  approach each other, collide and acquire real parts of the opposite sign. This is a hamiltonian Hopf bifurcation. For  $h > 0.07749$ , the soliton  $\psi_-$  is prone to the oscillatory instability [22].

When a damping term is added to the equation, the two stationary solitons  $\psi_+$  and  $\psi_-$  persist and can form a variety of multisoliton bound states, or complexes [16, 23–25]. In the next subsection, we show that *undamped* directly driven solitons can also form stationary complexes. Some of these complexes are bound so tightly that the solution represents a single entity. To distinguish these objects from the solitons  $\psi_+$  and  $\psi_-$ , we will be referring to the  $\psi_+$  and  $\psi_-$  as the *simple* solitons.

## B. The twist solitons

In addition to the two simple solitons expressible in elementary functions, the stationary equation (15) has two localised solutions that cannot be constructed analytically. Unless  $h$  is extremely small, each of these

two solutions has the form of a single entity [Fig.2(a,b)] — a soliton whose phase does not stay constant but grows, monotonically, as  $x$  changes from large negative to large positive values. When visualised in the three-dimensional  $(x, \text{Re}\psi, \text{Im}\psi)$ -space, it looks like a twisted ribbon (twisted by  $360^\circ$ ); hence we will be calling these two solutions simply “twists”. For the reason that will become obvious in the paragraph following the next one, we denote the two solutions  $\psi_{T_2}$  and  $\psi_{T_3}$ , respectively.

The twist solitons were previously encountered in the parametrically driven (undamped) nonlinear Schrödinger equation [32]. For each  $h$ , the parametrically driven twist is a member of a two-parameter family of stationary *two*-soliton solutions. The first parameter is the overall translation of the complex; the second one is the separation distance between the two bound solitons. The twist corresponds to a very small separation, where the two simple solitons bind to form a single entity. (The resulting object does not have even a slightest reminiscence of a two-soliton state; without knowing the whole family, the relation would hardly be possible to guess.)

The two simple solitons,  $\psi_+$  and  $\psi_-$ , detach from the  $U(1)$ -symmetric family of solitons of the unperturbed nonlinear Schrödinger at  $h = 0$  [21]. The two twist solutions of (15) also hail from the solitons of the unperturbed equation; however this time the relation is more complicated. Reducing  $h$ , the two solutions transform into complexes of well-separated solitons [Fig.2(c,d)]. Namely, one of the two twist solutions becomes a complex of two solitons:

$$\psi_{T_2} \rightarrow e^{3i\pi/4} \text{sech}(x + x_0) + e^{-3i\pi/4} \text{sech}(x - x_0),$$

where  $x_0 \rightarrow \infty$  as  $h \rightarrow 0$ . The other twist continues to a complex of *three* unperturbed solitons:

$$\psi_{T_3} \rightarrow i \text{sech}(x + x_0) - \text{sech}x - i \text{sech}(x - x_0),$$

and again, the separation  $x_0$  grows without bound as  $h \rightarrow 0$ . The “full names” of the two twists,  $\psi_{T_2}$  and  $\psi_{T_3}$ , were coined to reflect this multisoliton ancestry.

Despite being quiescent, nonpropagating objects, the twists carry nonzero momentum. Since equation (15) is invariant under the space inversion, the twist soliton with momentum  $P$  has a partner with momentum  $-P$  which is obtained by changing  $x \rightarrow -x$ . This transformation leaves the absolute value of  $\psi(x)$  intact but changes the sign of the phase derivative,  $(d/dx)\arg \psi(x)$ . By analogy with the right-hand rule of circular motion, the twist whose phase decreases as  $x$  grows from  $-\infty$  to  $+\infty$  [that is, the trajectory on the  $(\text{Re}\psi, \text{Im}\psi)$  phase plane is traced clockwise], will be called right-handed. The twist with the increasing phase (i.e. with a trajectory traced counter-clockwise) will be called left-handed. One can readily verify that the left-handed twist has a positive momentum, whereas the right-handedness implies  $P < 0$ .

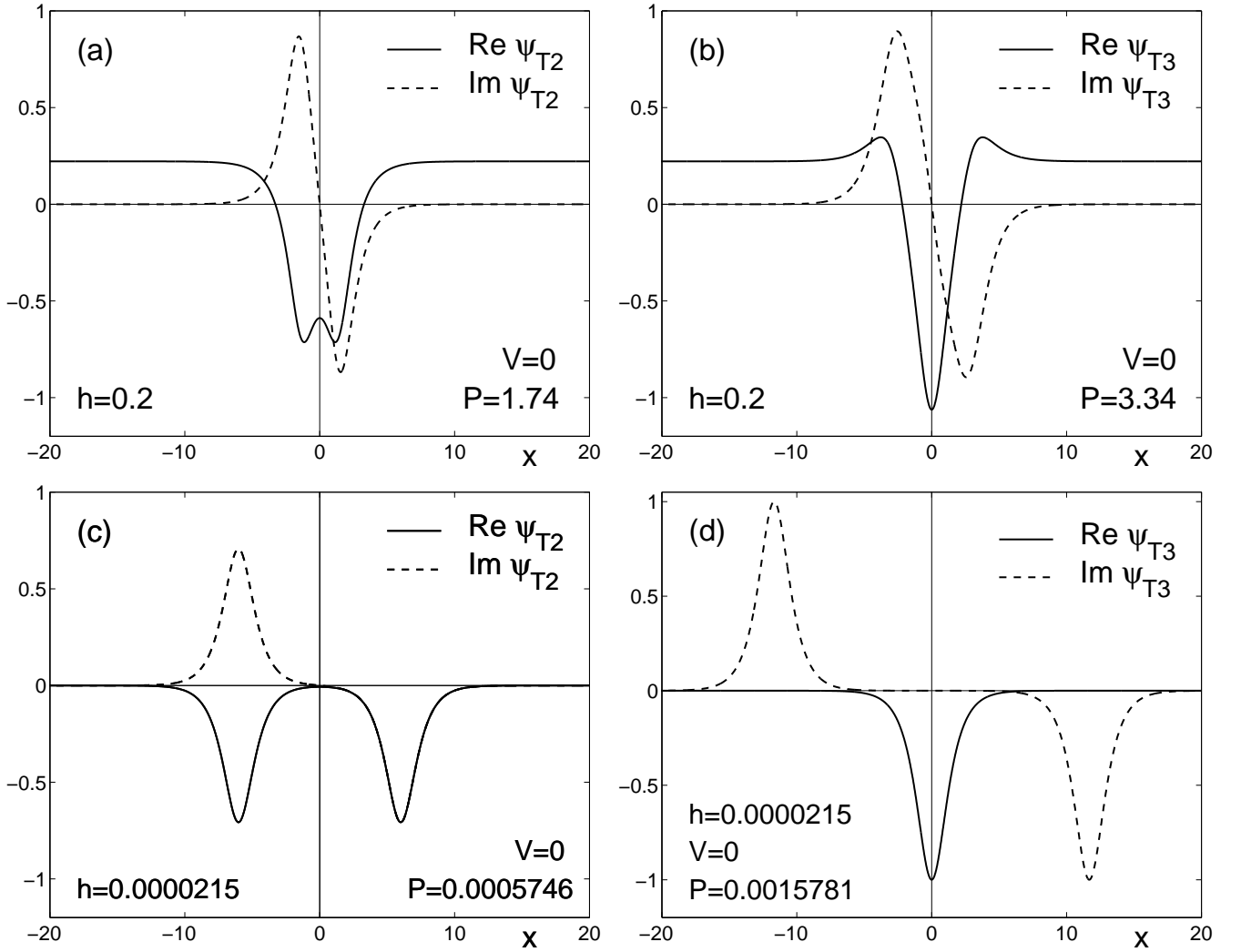


FIG. 2. (a,b): The two nonpropagating twist solutions for  $h \sim 1$ . (Here  $h = 0.2$ ). (c,d): The corresponding quiescent solutions when continued to an exponentially small  $h$ . (Here  $h = 2.15 \times 10^{-5}$ ). All twist solutions shown in these figures are left-handed.

Consider some particular value of the driving strength,  $h = h_0$ . Unlike the twist solution in the *parametrically* driven NLS, the *directly* driven twist with  $h = h_0$  is a member of a one-parameter (rather than two-parameter) family of solutions. (The only free parameter is the translation,  $-\infty < \theta < \infty$ , whereas the intersoliton separation  $\chi$  is fixed by  $h$ .) This can be concluded from the fact that the corresponding operator  $\mathcal{H}$  has only one, translational, zero eigenvalue. Had the twist been a member of a family of solutions parametrised by two continuous parameters, say  $\theta$  and  $\chi$ , the operator  $\mathcal{H}$  would have had an additional zero eigenvalue with the eigenvector  $\vec{\Psi}_\chi$ .

Letting  $\psi = x_1 + ix_2$ , the stationary equation (15) can be written as a classical mechanical system on the plane, with the Lagrangian

$$L = \frac{1}{2}(\dot{x}_1^2 + \dot{x}_2^2) - \frac{1}{2}(x_1^2 + x_2^2)^2 + \frac{1}{2}(x_1^2 + x_2^2) - hx_1.$$

The existence of a one-parameter family of homoclinic orbits  $\vec{x} = \vec{x}_\chi(t)$ , where  $\vec{x} \equiv (x_1, x_2)$ , would imply that the above system has the second integral of motion, in addition to the energy. However, equation (15) is known not to have any additional conserved quantities [34].

Finally, we need to comment on the stability of the two twist solutions. When  $h$  is equal to 0 and the two solutions represent a doublet and a triplet of infinitely separated solitons of the unperturbed nonlinear Schrödinger, the symplectic spectrum includes 8 and 12 zero eigenvalues, respectively. When  $h$  is small nonzero, only two eigenvalues remain at the origin in each case. In addition, the spectrum of the  $\psi_{T2}$  twist includes a complex quadruplet  $\pm\lambda, \pm\lambda^*$  and a pair of opposite pure imaginary eigenvalues. As  $h$  is increased, the imaginary pair collides with another imaginary pair emerging from the continuum, producing the second complex quadruplet. The spectrum of the  $\psi_{T3}$  twist includes two complex

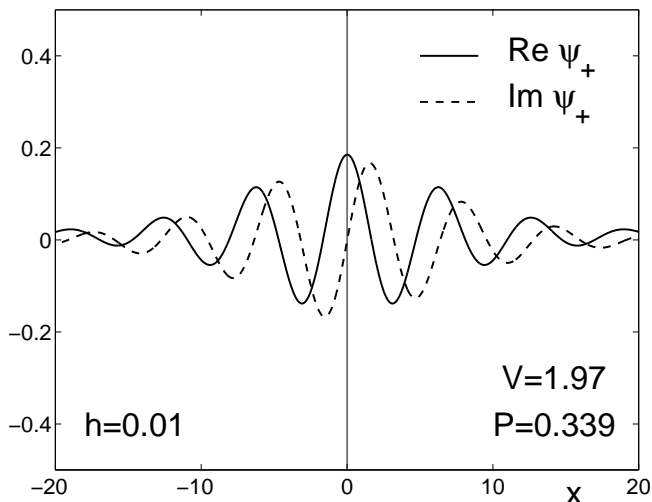


FIG. 3. As  $V \rightarrow c$ , the  $\psi_+$  solitons (for all  $h$ ) and  $\psi_-$  solitons (for small  $h$ ) approach linear waves with slowly decaying envelopes. Shown is the  $\psi_+$  solution with  $V$  close to  $c$ . (In this plot,  $h = 0.01$ ; the corresponding  $c = 1.9996$ .) The  $\psi_-$  solutions with  $V$  close to  $c$  have a similar shape.

quadruplets and a pair of pure imaginary eigenvalues; this arrangement remains in place for all  $h$ , from very small to  $h = \sqrt{2/27}$ . The bottom line is that both twist solutions are unstable for all  $h$ ; the instability is always of the oscillatory type.

## V. NUMERICAL CONTINUATION OF SIMPLE SOLITONS

### A. The travelling $\psi_+$ soliton

Travelling solitons are sought as solutions of the ordinary differential equation (9) under the boundary conditions  $\psi_\xi \rightarrow 0$  as  $|\xi| \rightarrow \infty$ .

We begin with the continuation of the quiescent soliton

### B. The travelling $\psi_-$ soliton; $h < 0.06$

In the case of the  $\psi_-$  solitons, there are two characteristic scenarios. When  $h$  lies between 0 and 0.06, the soliton  $\psi_-$  exists for all  $V$  between 0 and  $c$ . As  $V$  is increased from zero, the momentum  $P$  grows from  $P = 0$  and reaches its maximum at some point  $V_c$ ,  $0 < V_c < c$ . As  $V$  is changed from  $V_c$  to  $c$ , the momentum decays to zero [see Fig.4(a)]. On the other hand, when  $h$  equals 0.06 or lies above this value, the curve  $P(V)$  does not exhibit a point of maximum.

Consider, first, the case  $h < 0.06$ . The transformation scenario here is similar to the case of the soliton  $\psi_+$ ; see Fig.4. What makes the bifurcation curves for the  $\psi_+$

$\psi_+$ . For a sequence of  $h$  sampling the interval  $(0, \sqrt{2/27})$ , the branch starting at  $\psi_+$  was path followed all the way to  $V = c$ , where  $c$  is given by Eq.(8). As  $V$  increases, the amplitude of the solution decreases while the width grows. A typical solution with  $V$  close to  $c$  is shown in Fig.3. As  $V \rightarrow c$ , the momentum  $P$  tends to zero.

The resulting  $P(V)$  diagram is shown in Fig.4(a). For each  $h$ , the unstable stationary  $\psi_+$  soliton remains unstable when travelling sufficiently slow. The instability is due to a real eigenvalue  $\lambda > 0$  of the linearised operator (11).

As  $V$  grows, the unstable eigenvalue moves towards the origin along the real axis. Eventually, as the momentum  $P$  reaches its maximum, the positive eigenvalue  $\lambda$  collides with its opposite partner  $\lambda' = -\lambda$ , after which both real eigenvalues move onto the imaginary axis and the soliton acquires stability. The soliton remains stable all the way from the point  $V_c$ , where the momentum is maximum, to the value  $V = c$  where  $P = 0$  and the soliton ceases to exist.

The resulting  $P(V)$  dependence shows a remarkable similarity to the  $P(V)$  diagram [32] for the *parametrically* driven nonlinear Schrödinger,

$$i\psi_t - iV\psi_\xi + \psi_\xi\xi + 2|\psi|^2\psi - \psi = h\psi^*. \quad (17)$$

The “parametrically driven” diagram is reproduced in Fig.4(b) for the sake of comparison. One should keep in mind here that the notation used for the parametrically driven solitons is opposite to the notation employed in the externally driven situation. Thus, the parametrically driven stationary ( $V = 0$ ) soliton with a positive symplectic eigenvalue in its spectrum is denoted  $\psi_-$  (and not  $\psi_+$  as its externally driven counterpart). On the other hand, the parametrically driven stationary soliton denoted  $\psi_+$  is stable for sufficiently small  $h$  (like the externally driven soliton  $\psi_-$ ). For this reason, the objects featuring  $P(V)$  diagrams similar to those of our externally driven solitons  $\psi_+$ , are the parametrically driven solitons  $\psi_-$ .

and  $\psi_-$  solitons different, is the stability properties of the two solutions. Unlike the  $\psi_+$  solution, the *stationary*  $\psi_-$  soliton with  $h \leq 0.07749$  is stable and its stability persists when it is continued to small nonzero velocities. As  $V$  grows to the value  $V_c$  where the momentum reaches its maximum, two opposite pure imaginary eigenvalues collide at the origin on the  $(\text{Re}\lambda, \text{Im}\lambda)$  plane and cross to the positive and negative real axis, respectively. For the driving strengths  $h \leq 0.055$ , this implies the loss of stability.

As for the interval  $0.0551 \leq h \leq 0.06$ , here the instability sets in earlier, as  $V$  reaches some  $V = V_0$  (where  $V_0 < V_c$ ). At the point  $V = V_0$ , two pairs of pure imaginary eigenvalues collide and produce a quadruplet of complex

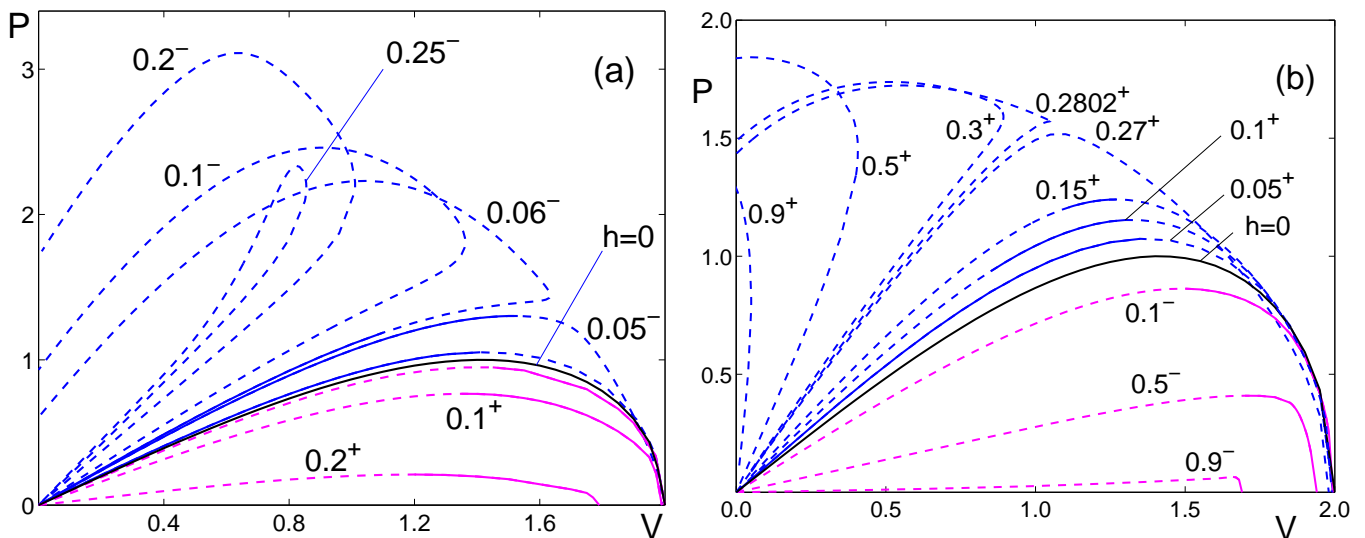


FIG. 4. (a) The momentum of the  $\psi_+$ ,  $\psi_-$  solitons continued to positive velocities. Decimal fractions attached to branches label the corresponding values of  $h$ , with the superscripts  $+$  and  $-$  indicating the  $\psi_+$  and  $\psi_-$  solitons. (For example,  $0.1^+$  marks the branch emanating from the stationary  $\psi_+$  soliton with  $h = 0.1$ .) The only two branches that have not been labelled are the  $\psi_+$  and  $\psi_-$  branches with  $h = 0.01$ ; the curve just above  $h = 0$  is  $0.01^-$  and the curve just below the  $h = 0$  branch is  $0.01^+$ . Solid curves mark stable and dashed ones unstable branches. (b) The corresponding  $P(V)$  diagram for the travelling parametrically driven solitons from [32].

eigenvalues  $\pm\lambda, \pm\lambda^*$ . (Here  $\lambda$  has a small real and finite imaginary part.) This is a point of the hamiltonian Hopf bifurcation, associated with the oscillatory instability [31, 32]. As  $V$  is increased to  $V_1$  (where  $V_0 < V_1 < V_c$ ), two pairs of complex-conjugate  $\lambda$  converge on the real axis, becoming two positive ( $\lambda_1 = \lambda_2 > 0$ ) and two negative ( $-\lambda_1 = -\lambda_2$ ) eigenvalues. Finally, when  $V$  crosses through  $V_c$ , the eigenvalues  $\lambda_1$  and  $-\lambda_1$  move on to the imaginary axis. The soliton does not restabilise at this point though; the real pair  $\pm\lambda_2$  persists for all  $V \geq V_c$ .

The bifurcation values  $V_0$  and  $V_1$  are, naturally, functions of  $h$ . The value  $V_0$  decreases (and  $V_1$  increases) as  $h$  is increased from 0.0551. Eventually, when  $h$  reaches 0.07749,  $V_0$  reaches zero. It is interesting to note that there is a gap between  $V_1$  and  $V_c$  for all  $h$ . Therefore the oscillatory and nonoscillatory instability coexist for no  $V$ ; for smaller  $V$  ( $V_0 < V < V_1$ ) the instability is oscillatory whereas for larger  $V$  ( $V > V_1$ ) the instability has a monotonic growth.

Finally, it is appropriate to mention here that the bifurcation curve for the  $\psi_-$  solitons with small  $h < 0.06$  has the same form as the  $P(V)$  dependence for the small- $h$  parametrically driven solitons (more specifically, parametrically driven  $\psi$ -plus solitons) — see Fig.4(b).

### C. The travelling $\psi_-$ soliton; $h \geq 0.06$

The  $P(V)$  graphs for  $h \geq 0.06$  are qualitatively different from the small- $h$  bifurcation curves. For these larger  $h$ , the bifurcation curve emanating from the origin on

the  $(V, P)$ -plane turns back at some  $V = V_{\max}$ , with the derivative  $\partial P / \partial V$  remaining strictly positive for all  $V \leq V_{\max}$ .

For  $h$  in the interval  $0.06 \leq h < 0.25$ , the  $P(V)$  curve crosses the  $P$ -axis [Fig.4(a), Fig.5]. The solution arising at the point  $V = 0$  is nothing but the  $\psi_{T2}$  twist soliton, shown in Fig.2(a).

As we continue this branch to the  $V < 0$ -region, the twist transforms into a complex of two well-separated  $\psi_-$  solitons. The  $P(V)$  curve makes one more turn and eventually returns to the origin on the  $(V, P)$ -plane (Fig.5). As  $V$  and  $P$  approach zero, the distance between the solitons in the complex tends to infinity.

An interesting scenario arises when  $h$  is greater or equal than 0.25. Here, as  $V$  grows from zero, the soliton  $\psi_-$  gradually transforms into a three-soliton complex  $\psi_{(-++)}$ . The branch turns back towards  $V = 0$  but does not cross the  $P$ -axis. Instead of continuing to negative  $V$ , the branch reapproaches the origin in the  $(V, P)$  plane, remaining in the positive  $(V, P)$  quadrant at all times. The ingoing path is almost coincident with the outgoing trajectory; as a result, the branch forms a lasso-looking loop [Fig.4(a)].

Turning to the stability properties of solutions along the branch continued from  $\psi_-$ , we start with a short interval  $0.06 \leq h \leq 0.07749$ . The movements of the stability eigenvalues along the section of the curve emanating from the origin on the  $(V, P)$  plane, are similar to the interval  $0.055 < h < 0.06$  that we discussed in the previous paragraph. The stationary  $\psi_-$  soliton is stable and stability persists for small  $V$ . As  $V$  reaches a certain  $V_0 > 0$ ,





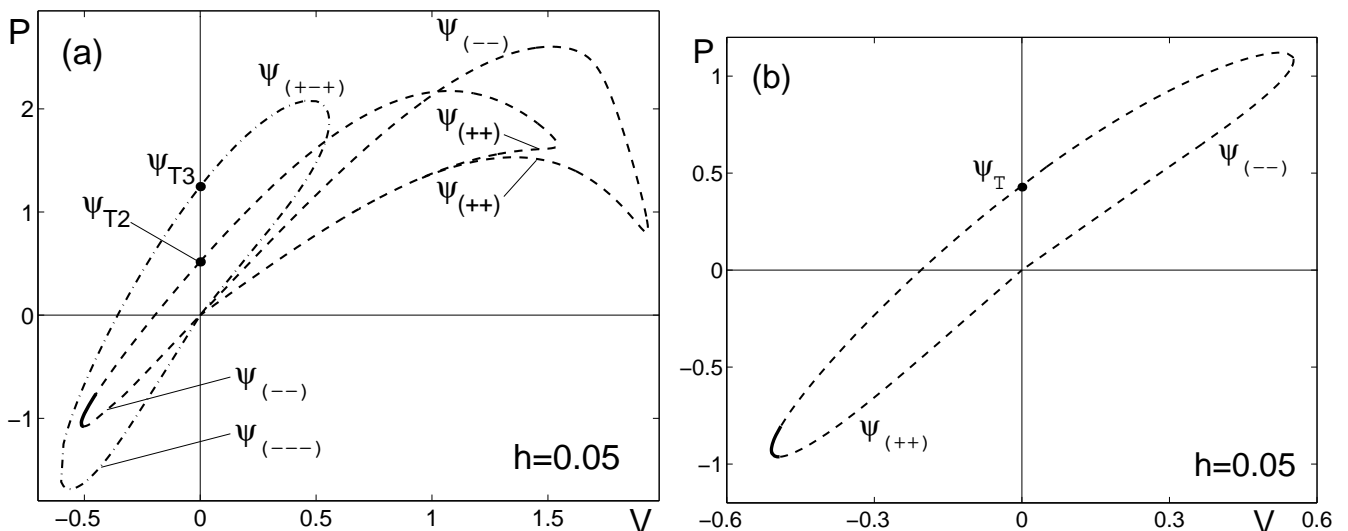


FIG. 6. (a) Continuation of the  $T2$  and  $T3$  twist solutions in the case of small  $h$ . Also shown is the two-soliton branch which connects the origin to itself without intersection the vertical axis. (b) The continuation of the twist soliton in the case of the parametrically driven NLS equation (adapted from [32]). More solution branches can be obtained by the reflection  $V \rightarrow -V$ ,  $P \rightarrow -P$  both in (a) and (b).

### B. Travelling twist $T3$ , $h < 0.25$

Figs.6(a) and 5 also show the continuation of the  $T3$  twist soliton. The bifurcation diagrams obtained for  $h < 0.06$  and  $0.06 \leq h < 0.25$  are qualitatively similar.

Continuing the stationary  $T3$  to positive velocities, the solution transforms into a  $\psi_{(+-)}$  complex. If we, instead, continue to negative velocities, the twist transforms into a triplet of  $\psi_-$  solitons. Both  $V > 0$  and  $V < 0$  parts of the curve turn and connect to the origin on the  $(V, P)$  plane. As  $V$  and  $P$  approach the origin on either side, the distance between the three solitons bound in the complex grows without limit.

The stationary  $T3$  has two complex quadruplets in its spectrum; depending on  $h$ , both or one of these converge on the real axis as we continue it to  $V > 0$  and  $V < 0$ . Two opposite eigenvalues cross through  $\lambda = 0$  at the extrema of  $P(V)$ . Finally, as  $V$  and  $P$  approach the origin, the spectrum transforms into the union of spectra of three separate solitons.

### C. Travelling twists $T2$ and $T3$ , $h \geq 0.25$

Another parameter region where the continuation of the  $\psi_-$  does not cross the  $P$ -axis, is  $h \geq 0.25$ . The result of the continuation of the two twist solutions is shown in Fig.7(a). The continuation of  $T2$  to the negative velocities proceeds according to scenario similar to  $h = 0.2$

and  $h = 0.05$ : the twist transforms into a complex of two solitons  $\psi_-$ . At some negative  $V$  the curve turns back and connects to the origin on the  $(V, P)$  plane, with the distance between the two solitons bound in the complex increasing without bound. The eigenvalues evolve accordingly: two complex quadruplets in the spectrum of the stationary  $T2$  persist for all  $V < 0$ , supplemented by a pair of real eigenvalues which arrive from the imaginary axis at the point of minimum of  $P(V)$ . As  $V, P \rightarrow 0$ , the discrete spectrum becomes the union of the eigenvalues of two simple solitons.

The continuation of  $T2$  to positive  $V$  produces a less expected outcome. Instead of turning clockwise and connecting to the origin as in Fig.6(a), the curve turns counterclockwise and crosses through the  $P$ -axis once again. The solution arising at the point  $V = 0$  is nothing but the twist  $T3$ . Two complex quadruplets in the spectrum of  $T2$  persist as it is continued to  $T3$ .

The subsequent continuation produces a hook-shaped curve similar to the curve described in the previous paragraph and leading to the origin on the  $(V, P)$ -plane. The corresponding solution is a complex of three  $\psi_-$  solitons, shown in Fig.7(b). The third complex quadruplet emerges at some  $V$  before the turning point, and a pair of opposite real eigenvalues arrives from the imaginary axis at the point of minimum of the momentum. As  $V, P \rightarrow 0$ , the distance between the solitons grows to infinity and the spectrum approaches the union of the eigenvalues of three separate solitons  $\psi_-$ .

### D. Other branches

It is appropriate to note that there are branches which do not originate on any of the four stationary solutions

listed above ( $\psi_{\pm}$ ,  $\psi_{T2}$  or  $\psi_{T3}$ ). The simplest of these

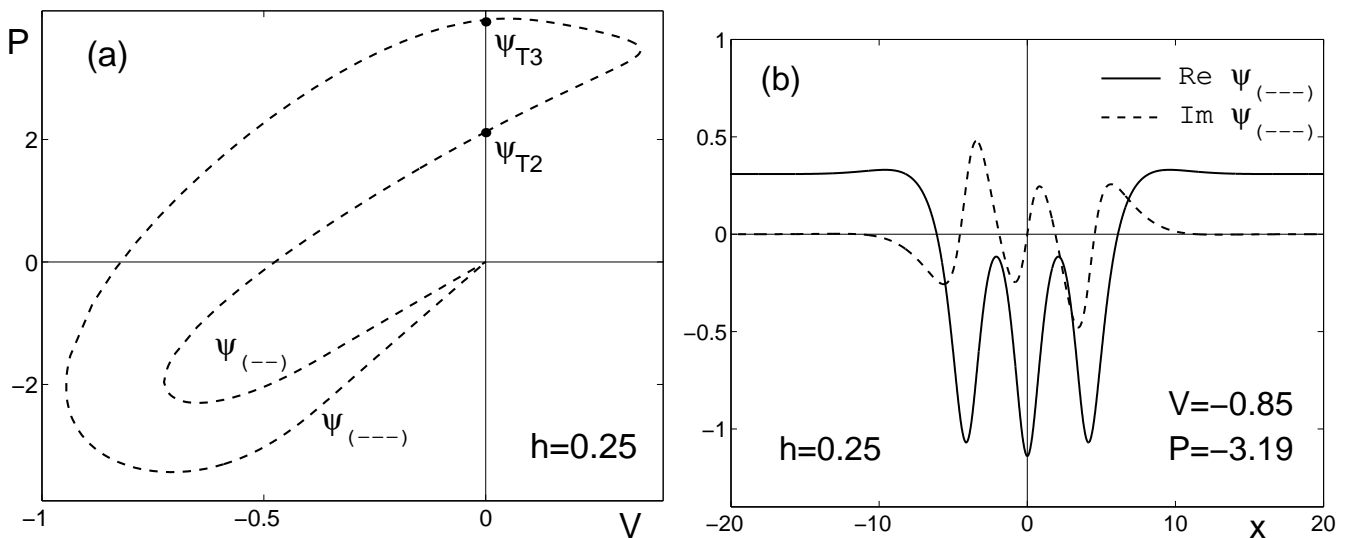


FIG. 7. (a) The  $P(V)$  curve resulting from the continuation of the twist for  $h = 0.25$ . The starting point of the continuation is marked by an open circle. All branches shown in this figure are unstable. (b) A  $\psi_{(---)}$  solution on the lower branch in (a). Here  $V = -0.85$ ,  $P = -3.2$ . In (b), the solid lines show the real and dashed imaginary part.

emerge from the origin on the  $(V, P)$  plane as bound states of simple solitons with large separation. One branch of this sort arises for  $h \geq 0.06$  (Fig. 5). It emerges from the origin as the  $\psi_{(++)}$  and returns as the  $\psi_{(++++)}$  complex. The entire branch is unstable.

Next, unlike in the parametrically driven NLS, the same pair of *externally* driven travelling solitons may bind at various distances. In particular, when  $h$  is smaller than 0.06, there is more than one bound state of two  $\psi_+$  solitons and more than one complex of two  $\psi_-$  solitons. Fig.6(a) shows a branch  $\psi_{(-)}$  that emerges from the origin in the first quadrant of the  $(V, P)$  plane, describes a loop and re-enters the origin — this time as a  $\psi_{(++)}$  branch. Note that for small  $V$  and  $P$ , the re-entering  $\psi_{(++)}$  branch is indistinguishable from the other  $\psi_{(++)}$  branch — the one that continues from the twist solution. (In a similar way, the  $V \rightarrow -V$ ,  $P \rightarrow -P$  reflection of the  $\psi_{(-)}$  branch overlaps with the small- $V, P$  section of the  $\psi_{(-)}$  branch arriving from the twist.) All solutions constituting this branch are unstable.

## VII. CONCLUDING REMARKS

In this paper, we studied stationary and moving solitons of the externally driven nonlinear Schrödinger equation,

$$i\psi_t + \psi_{xx} + 2|\psi|^2\psi - \psi = -h. \quad (18)$$

Our continuation results are summarised in Fig.8(a) which shows ranges of stable velocities for each value of the driving strength  $h$ .

The notation  $\psi_+$  and  $\psi_-$  in this figure is used for the travelling waves obtained by the continuation of the sta-

tionary  $\psi_+$  and  $\psi_-$  solitons, respectively. The travelling soliton preserves some similarity with its stationary ancestor; this justifies the use of the same notation.

The uppermost curve in this figure is given by  $V = c(h)$  where  $c$  is the maximum velocity of the soliton propagation, Eq.(8). This curve serves as the upper bound of the travelling  $\psi_+$  soliton existence domain. The dotted curve demarcates the existence domain of the travelling  $\psi_-$  soliton. For  $h$  between 0 and 0.06 it coincides with the  $V = c$ ; for  $0.06 \leq h \leq 0.2722$  it is given by  $V = V_{\max}(h)$  where  $V_{\max}$  is the position of the turning point in Fig.4(a).

The area shaded in blue (light grey) gives the stability region of the soliton  $\psi_+$  and the area shaded by purple (dark grey) is the  $\psi_-$  stability domain. Note that the blue and purple regions partially overlap: for small  $h$ , there is a range of “stable” velocities accessible to solitons of both families. The light (yellow) strip inside the purple (dark grey) region represents the stability domain of the bound state of two  $\psi_-$  solitons.

As we cross the right-hand “vertical” boundary of the purple (dark grey) region, the  $\psi_-$  soliton loses its stability to an oscillatory mode. If we had damping in the system, the onset of instability would correspond to the Hopf bifurcation giving rise to a time-periodic solution. In the absence of damping, the oscillatory instability produces an oscillatory structure with long but finite lifetime [31]. These solitons with oscillating amplitude and width, travelling with oscillatory velocities, were observed in [30]. These are expected to exist to the right of the purple (dark grey) region.

Where possible, we tried to emphasise the similarity of the arising bifurcation diagrams with the corresponding diagrams for the *parametrically* driven nonlin-

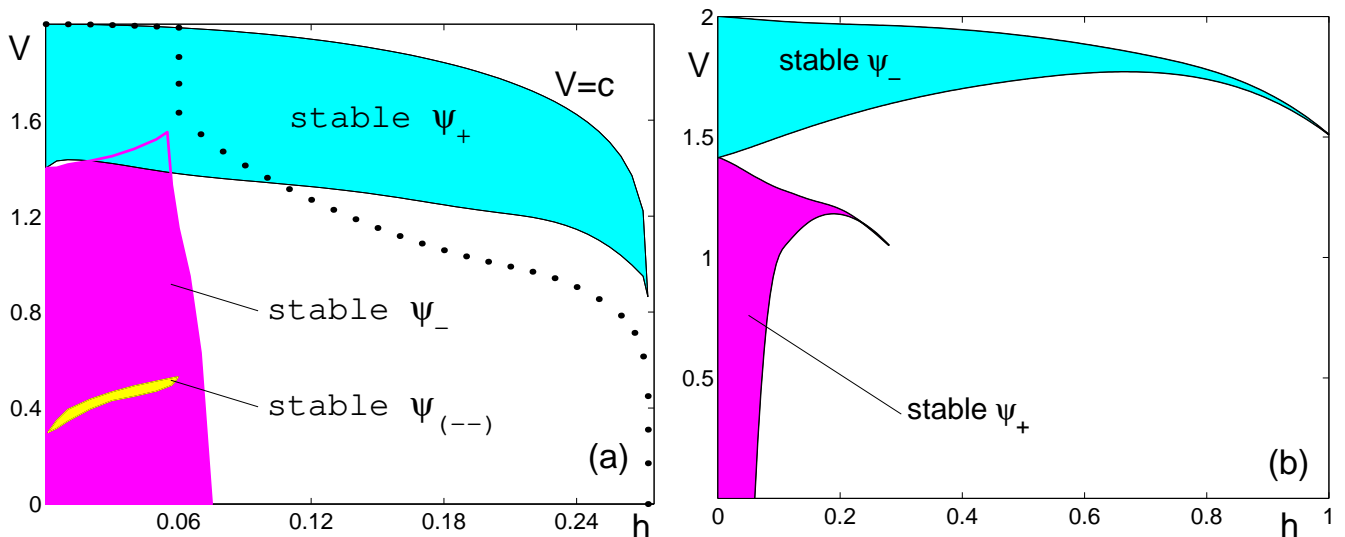


FIG. 8. (a) The chart of the stable one-soliton solutions of the externally driven nonlinear Schrödinger equation (18). Here  $h$  varies from 0 to  $\sqrt{2/27} \approx 0.2722$ . (b) The corresponding attractor chart for the parametrically driven soliton (adapted from [32]).

ear Schrödinger equation:

$$i\psi_t + \psi_{xx} + 2|\psi|^2\psi - \psi = h\psi^*. \quad (19)$$

Fig.8(b) reproduces the soliton attractor chart for Eq.(19) [32]. The structure of the stability regions in the two figures is remarkably similar. The slowly moving solitons in the purple- (dark grey-) tinted region inherit their

stability from the stationary solitons of the family which is stable for small  $h$  (the  $\psi_-$  family in the externally-driven and the  $\psi_+$  family in the parametrically-driven case). On the other hand, the solitons in the blue- (light grey-) shaded area are transonic (i.e. move close to  $c$ , velocity of the sound waves). Their stability is due to the proximity of the nonlinear Schrödinger equation to the KdV in the transonic limit [35].

- 
- [1] Y. Braiman, W. L. Ditto, K. Wiesenfeld, M. L. Spano, Phys. Lett. A **206** (1995) 54; Y. Braiman, J. F. Lindner, W. L. Ditto, Nature **378** (1995) 465; L. M. Floria, J. J. Mazo, Adv. Phys. **45** (1996) 505; A. Gavrielides, T. Kottos, V. Kovanis, G. P. Tsironis, Phys. Rev. E **58** (1998) 5529; R. Basu Takur, L. Q. English and A. J. Sievers, J. Phys. D: Appl. Phys. **41** 015503 (2008); J. Cuevas, L. Q. English, P. G. Kevrekidis, and M. Anderson, Phys. Rev. Lett. **102**, 224101 (2009)
  - [2] D. W. McLaughlin, A. C. Scott, Phys. Rev. A **18** (1978) 1652; J. C. Eilbeck, P. S. Lomdahl, A. C. Newell, Phys. Lett. A **87** (1981) 1; M. Salerno, A. C. Scott, Phys. Rev. B **26** (1982) 2474; F. If, P. L. Christiansen, R. D. Parmentier, O. Skovgaard, M. P. Soerensen, Phys. Rev. B **32** (1985) 1512; M. Fordsmand, P. L. Christiansen, F. If, Phys. Lett. A **116** (1986) 71.
  - [3] K. Maki, Phys. Rev. B **18** (1978) 1641; D. J. Kaup, A. C. Newell, Phys. Rev. B **18** (1978) 5162; D. Bennett, A. R. Bishop, S. E. Trullinger, Z. Phys. B **47** (1982) 265.
  - [4] R. Khomeriki, M. Abolfath, and K. Mullen, Phys. Rev. B **65** 121310(R) (2002)
  - [5] E. B. Volzhan, N. P. Giorgadze, A. D. Pataraya, Sov. Phys. Solid State **18** (1976) 1487; M. M. Bogdan, PhD thesis, Institute for Low Temperature Physics and Engineering, Kharkov, 1983; G. A. Maugin, A. Miled, Phys. Rev. B **33** (1986) 4830; A. M. Kosevich, B. A. Ivanov, A. S. Kovalev, Phys. Rep. **194** (1990) 118.
  - [6] G. J. Morales, Y. C. Lee, Phys. Rev. Lett. **33** (1974) 1016; A. V. Galeev, R. Z. Sagdeev, Yu. S. Sigov, V. D. Shapiro, V. I. Shevchenko, Sov. J. Plasma Phys. **1** (1975) 5
  - [7] K. Nozaki and N. Bekki, Physica D **21** 381 (1986)
  - [8] Lei Lin, C. Shu, G. Xu, J. Stat. Phys. **39** (1985) 633
  - [9] R. Khomeriki, S. Lepri, and S. Ruffo, Phys. Rev. E **64**, 056606 (2001); Physica D **168-169**, 152 (2002); T. Dauxois, R. Khomeriki, and S. Ruffo, Eur. Phys. J. Special Topics **147**, 3 (2007)
  - [10] G. Cohen, Phys. Rev. E **61**, 874 (2000)
  - [11] V. V. Vyas, T. S. Raju, C. N. Kumar, and P. K. Panigrahi, J. Phys. A: Math. Gen. **39**, 9151 (2006)
  - [12] L. Friedland, Phys. Rev. E **58**, 3865 (1998); S. V. Batalov, E. M. Maslov, and A. G. Shagalov, JETP **108** 890 (2009)
-

- [13] U Peschel, O Egorov, F Lederer, *Opt. Lett.* **29**, 1909 (2004); A V Gorbach, S Denisov, S Flach, *Opt. Lett.* **31**, 1702 (2006)
- [14] L. A. Lugiato and R. Lefever, *Phys. Rev. Lett.* **58**, 2209 (1987); W J Firth, G K Harkness, A Lord, J M McSloy, D Gomila, and P Colet, *J. Opt. Soc. Am. B* **19** 747 (2002)
- [15] M. Haeltermann, S. Trillo, S. Wabnitz, *Opt. Lett.* **17** (1992) 745; *Opt. Commun.* **91** (1992) 401;
- [16] S. Wabnitz, *Opt. Lett.* **18** (1993) 601; *J. Opt. Soc. Am. B* **13**, 2739 (1996)
- [17] G. M. Reznik and V. Zeitlin, *Phys Rev Lett* **99**, 064501 (2007); *Nonlin. Processes Geophys.* **16**, 381 (2009)
- [18] D. J. Kaup, A. C. Newell, *Proc. Roy. Soc. London Ser. A* 361 (1978) 413.
- [19] K Nozaki and N Bekki, *J. Phys. Soc. Japan* **54**, 2363 (1985); K. H. Spatschek, H. Pietsch, E. W. Laedke, Th. Eickermann, in: *St. Pnevmatikos, T. Bountis, Sp. Pnevmatikos* (Eds.), *Singular Behaviour and Nonlinear Dynamics*, *Proceedings of International Conference, Samos, 1988*, World Scientific, Singapore, 1989, p. 555; Th. Eickermann, R Grauer, K H Spatschek, *Phys Lett A* **198**, 383 (1995);
- [20] I V Barashenkov and Yu S Smirnov, *Phys Rev E* **54** 5707 (1996)
- [21] I V Barashenkov and E V Zemlyanaya, *Physica D* **132** 363 (1999)
- [22] I V Barashenkov, T Zhanlav and M M Bogdan, in: *Nonlinear World. IV International Workshop on Nonlinear and Turbulent Processes in Physics*. Kiev, October 1989. Edited by V G Bar'yakhtar, V M Chernousenko, N S Erokhin, A G Sitenko and V E Zakharov. World Scientific, Singapore, 1990, p.3
- [23] D Cai, A R Bishop, N Grønbech-Jensen, and B A Malomed, *Phys Rev E* **49**, 1677 (1994)
- [24] I V Barashenkov, Yu S Smirnov, N V Alexeeva, *Phys. Rev. E* **57**, 2350 (1998)
- [25] M. Kollmann, H. W. Capel, T. Bountis, *Phys. Rev. E* **60**, 1195 (1999)
- [26] H Konno and P S Lomdahl, *Phys Lett A* **193**, 35 (1994);
- [27] L Friedland and A G Shagalov, *Phys Rev Lett* **81** 4357 (1998); S G Glebov, O M Kiselev, V A Lazarev, *Proceedings of the Steklov Institute of Mathematics, Suppl.* **1**, S84 (2003); S Glebov, O Kiselev, *J. Nonlin. Math. Phys.* **12** 330 (2005); S. V. Batalov and A. G. Shagalov, to appear in *Phys Rev E* (2011)
- [28] G Terrones, D W McLaughlin, E A Overman, and A E Pearlstein, *SIAM J. Appl. Math.* **50**, 791 (1990)
- [29] J M Ghidaglia, *Ann. Inst. Henri Poincaré* **5** 365 (1988); *Math. Modelling and Numerical Analysis* **23** 433 (1989); E Shlizerman and V Rom-Kedar, *Chaos* **15** 013107 (2005); *Phys Rev Lett* **96** 024104 (2006);
- [30] F G Mertens, N R Quintero, A R Bishop, *Phys Rev E* **81**, 016608 (2001)
- [31] N V Alexeeva, I V Barashenkov, D E Pelinovsky, *Nonlinearity* **12**, 103 (1999)
- [32] I V Barashenkov, E V Zemlyanaya, M Bär, *Phys Rev E* **64**, 016603 (2001)
- [33] See Appendix A6 in V. I. Arnold, *Mathematical Methods of Classical Mechanics* (Graduate Texts in Mathematics) Springer-Verlag, New York, 1989.
- [34] J Hietarinta, *Phys Lett A* **96** 273 (1983)
- [35] I V Barashenkov and V G Makhankov, *Phys Lett A* **128**, 52 (1988)